Robotica (2013) volume 31, pp. 657–667. © Cambridge University Press 2012
doi:10.1017/S0263574712000641

Stiffness estimation of a parallel manipulator using image analysis and camera calibration techniques

Abraham Gonzalez-Hernandez* and Eduardo Castillo-Castaneda

Instituto Politecnico Nacional, CICATA Unidad Queretaro, Cerro Blanco 141, Colinas del Cimatario, 76090 Queretaro, Mexico

(Accepted October 1, 2012. First published online: November 19, 2012)

SUMMARY

This work presents a methodology using image analysis to estimate the experimental stiffness of a parallel robot, Parallix LKF-2040, a 3-degree-of-freedom manipulator. The proposed methodology has a simple implementation and can be applied to different architectures of parallel robots. This methodology uses image analysis and camera calibration techniques to estimate compliant displacements of mobile platform produced by several loads at the end effector level, and calculate stiffness in a specific position of mobile platform. Experimental results are presented for different positions within the workspace.

KEYWORDS: Stiffness; Parallel manipulator; Camera calibration; Image analysis.

1. Introduction

Stiffness is an important feature to evaluate the performance of a robot manipulator, since the forces present on its elements can produce significant compliant displacements. Such types of displacements considerably reduce positioning accuracy of a robot. High stiffness is a characteristic often associated with parallel manipulators,[2] since more than two limbs are supporting the load, as the Gough–Stewart platform with six limbs attached to a mobile platform.

In 1990, Gosselin[3] conducted relevant studies about stiffness in parallel manipulators. In that work, an analytical method is presented to find stiffness maps for planar and spatial manipulators with 3 degrees-of-freedom (DOF). Gosselin affirms that stiffness, for a specific position in the workspace, can be characterized by the stiffness matrix and can be estimated through Jacobian matrix.

Clinton and Zhang[4] in 1997 proposed a mathematical model describing the stiffness of a milling machine based on the Gough–Stewart platform. The model is based on structural matrix analysis to obtain stiffness matrix of each mechanical element, and then assemble them in the stiffness matrix of the whole system; the method assumes that elements have only linear deformations. They also performed an experimental analysis based on the stiffness test for machining centers using ASME B5.54 standard.

In 2000, Rebeck and Zhang[5] presented a method to evaluate the stiffness of links, joints, and fixed platform of a milling machine based on the Gough–Stewart platform; the stiffness of these elements was estimated using the principle of virtual work. Their work considered that compliant displacements were additive, then stiffness was the sum of the stiffness of fixed platform and links.

In 2001, Huang *et al.*[6] presented a two-step approach to estimate the stiffness of TRIPOD, a parallel kinematic machine. The first step decomposes the machine structure in two substructures; the stiffness model of both substructures was formulated following the principle of virtual work. The second step estimates the stiffness model of whole machine applying the principle of linear superposition.

Ceccarelli and Carbone presented[7] the stiffness analysis of robots, CaPaMan and CaHyMan.[8] The stiffness matrix is deduced from the stiffness of the most important mechanical parts such as speed reducer elements and robot legs.

In 2003, Yoon *et al.*[9] presented a method to analyze the stiffness of links and joints based on the elastic deformation theory.

In 2005, Ceccarelli and Carbone[10] proposed a simple approach to estimate coefficients of stiffness matrix of parallel manipulators that only considered the displacements caused by the application of linear forces. The compliant displacements are measured using the Milli-CATRASYS, a system to measure the mobile platform-compliant displacements caused by applying a known load. Milli-CATRASYS is an array of six sensors LVDT fixed in a framework different from robot base but linked to the mobile robot platform through six retractable cables. The cable length (measured by LVDTs) changes according to the applied forces. The inverse kinematics of the sensor array allows finding the pose of mobile platform for each load.

In 2005, Company *et al.*,[11] working with the parallel manipulator H4, presented a method considering links as springs to simplify the stiffness model. Corradini *et al.*[12] used three-dial test indicators to measure compliant displacements of mobile platform of a 4-DOF parallel manipulator. The dials are reset to zero without load and display the end-effector displacement on each axis when a known load is applied. Since compliant displacements and forces are known, the experimental stiffness matrix can be determined numerically.

In 2006, Deblaise *et al.*[13] presented a novel analytical approach to calculate the stiffness matrix of parallel robots based on matrix structural analysis; the stiffness matrix is obtained and can be considered in the controller to improve accuracy of a robot.

* Corresponding author. E-mail: ecastillo@ipn.mx

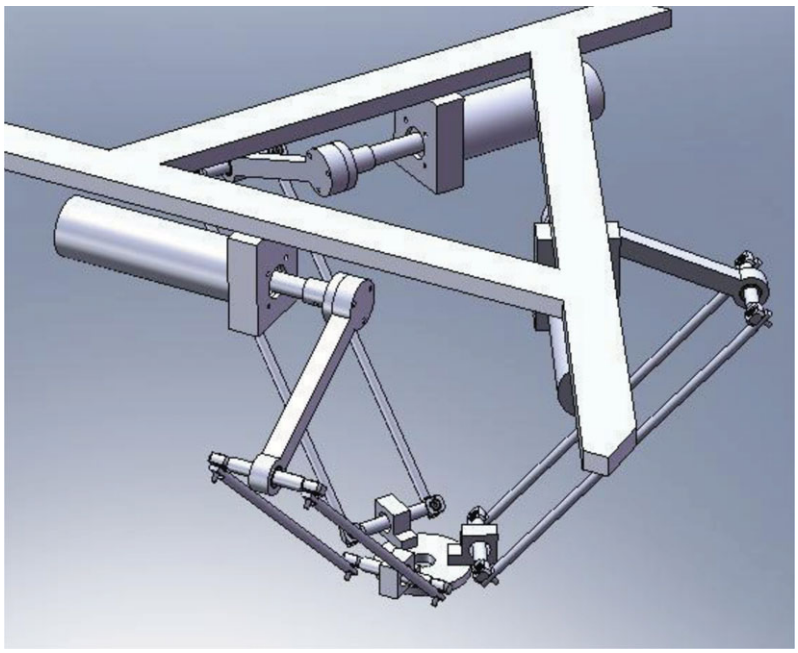

Fig. 1. (Colour online) The Parallix LKF-2040 robot.

In 2008, Majou *et al.*[14] presented a parametric stiffness analysis applied to manipulator Orthoglide. This method is based on a lumped parameter model of a flexible link that replaces the links for virtual joints and virtual rigid links.

In 2008, Goncalves and Carvalho[15] presented a method based on structural analysis to obtain the stiffness matrix of a 6-RSS manipulator; the results are compared with those obtained with Finite Element Analysis (FEA).

In 2009, Pashkevich *et al.*[16] presented a method to evaluate stiffness based on a model of multidimensional global parameters that replaces flexible links by 6-DOF virtual springs that describe position and orientation.

In 2009, Najera *et al.*[17] estimated the stiffness of a 6-RUS manipulator based on Ceccarelli and Carbone's proposed approach.[10] The stiffness of connecting rods and cranks of a parallel manipulator were calculated using FEA, and the stiffness of a speed reducer was determined experimentally. This work emphasizes that the maximum values of stiffness are presented in stationary configurations.

Lang *et al.*'s[18] work presents a technique to obtain a deformation model of an object described by a discrete Green's functions matrix based on its deformation behavior. The object deformations are measured with a trinocular stereo-head, while multiple loads are applied with a robot arm; both estimated deformation and force are recorded at high rates. Although in their work the stiffness of a robot or an object is not measured, it contains all theoretical and practical elements to perform it.

The work presented in this paper describes a methodology to experimentally estimate the stiffness of a parallel manipulator, Parallix LKF-2040,[1] using computer vision techniques. The stiffness matrices are obtained for a subset of positions within the workspace. The main contribution of this work is the method that measures compliant displacement in three dimensions (3D), including changes in orientation, when an external force is applied. The obtained displacement measurements are used to evaluate the stiffness of a manipulator. One important advantage of this method is that it is possible to measure stiffness at any point of the whole workspace of a robot. The accuracy of this method depends on the quality of machine vision system, that is, on camera calibration technique and camera resolution. The software used in this work is based on MATLAB ToolBox "Camera Calibration Toolbox"; camera resolution is 2592×1944 pixels, which allows to ensure enough accuracy for such kind of robot-compliant displacements. A 3D graphical representation of manipulator stiffness is generated using the value of the stiffness matrix determinant for each position.

2. Description of Experimental Set Up

2.1. Parallix LKF-2040 robot

The Parallix LKF-2040 robot (see Fig. 1) is a pure translational manipulator-type Delta. The actuators are mounted on a fixed platform and the end-effector is mounted on a mobile platform. The workspace is larger than the Delta-type robot, since two rotational joints replaced spherical joints. The structure of the manipulator is light, simplifying the dynamics and minimizing the displaced load. The robot is currently used for teaching purposes since it has an open architecture. Each kinematic chain has three rotational joints, two of these are passives joints.

The fixed platform is made of square steel tube. The actuators are servomotors MAXON model RE-35, 90 W and 24 V DC with planetary gears and incremental encoders. The servomotors are mounted on the fixed platform through aluminum nuts. The upper links are made of aluminum and are attached to motors through stainless steel couplings. The lower links are constructed of round tubing. The passive

https://doi.org/10.1017/S0263574712000641 Published online by Cambridge University Press

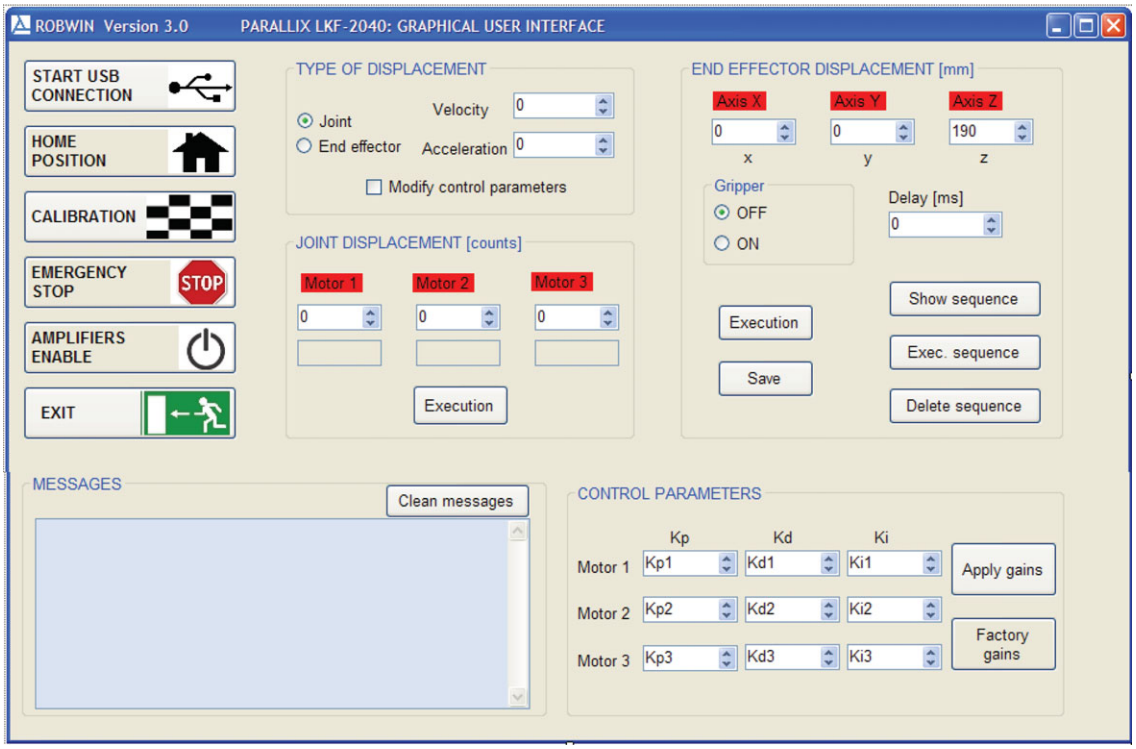

Fig. 2. (Colour online) ROBWIN version 3.0: Graphical user interface.

joints are commercial needle bearings and are mounted on stainless steel shafts. The mobile platform is made of aluminum. The displacements in the Cartesian space are done through motion control boards type PIC-SERVO SC using ROBWIN Version 3.0, a Graphical User Interface programmed in Visual C++ under Windows. Figure 2 shows the main window of ROBWIN Version 3.0.

2.2. The USB camera

Our approach needs images from patterns fixed to the mobile and fixed platforms. A color camera, type USB from Imaging Source, model DFK 72UC02 with 2592×1944 pixels resolution, was used to acquire images. The camera was placed in front of the robot, far enough to keep the patterns inside the camera field of view and to get a convenient ratio pixel/millimeter.

2.3. Patterns for camera calibration

Two planar checkerboards with 1×1 cm squares were used as reference patterns. The first pattern (rectangular shape) was located on the fixed platform (on one motor support; see Fig. 3). This pattern was used to determine transformation matrix between the camera frame and the robot frame. The second pattern (square shape) was located on mobile platform (see Fig. 3). This pattern was used to determine compliant displacement caused by the application of a known load at the end-effector level.

2.4. Device to apply known forces

A special device was built to apply forces on X and Y-axes of the mobile platform (see Fig. 4). The device was mounted on a tripod to move it into the robot workspace. The forces are applied using standard mass of 0.500, 0.200, and 0.100 kg. To apply forces on Z-axis, the load is applied directly on the mobile platform. The device was designed to ensure that forces are actually collinear to X and Y-axes of the mobile platform. The device is linked to the mobile platform by a wire only, which transfers the applied force having the effect of an external load. Friction was reduced by integrating pulleys with bearings to force transmission elements, and collinearity was guaranteed by integrating steel guides to align load axis with each axis of the mobile platform. However, friction force on the pulleys was experimentally estimated. We are assuming that true force applied to the mobile platform is the difference between the known force and the friction force. Then true force was measured by a dynamometer, which was placed between the pulley and the mobile platform. The true force was measured with a 5-g resolution dynamometer using an 8-mm circular cross-section belt for a 500-g load. For 10 repeated measurements, the friction force was 28 g with a standard deviation of 8 g; this value represents less than 6% of the applied force.

2.5. Software to estimate mobile platform-compliant displacements

For each known applied force, the compliant displacement of the mobile platform was estimated using camera calibration techniques. Using these techniques some parameters are estimated: intrinsic parameters of the camera (focal length, principal point, and distortion coefficients) and extrinsic parameters (position and orientation of the reference pattern). The software

https://doi.org/10.1017/S0263574712000641 Published online by Cambridge University Press

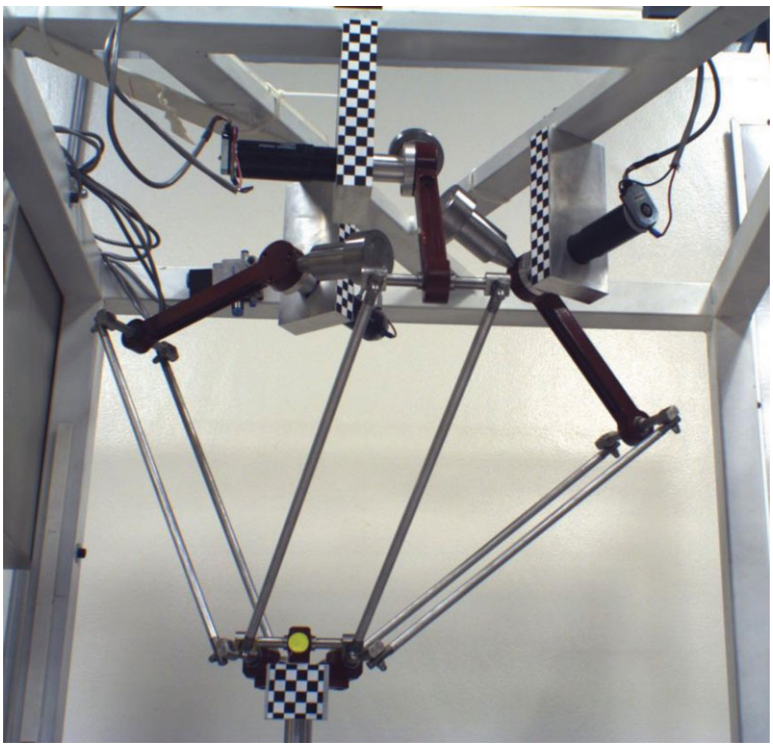

Fig. 3. (Colour online) Mobile and fixed reference patterns.

used in this work was based on MATLAB ToolBox "Camera Calibration Toolbox,"[19] some modifications were implemented to the software to estimate the displacements of the pattern and express them with respect to robot frame.

3. Methodology

3.1. Transformation between camera and robot frames

The method proposed in this work is to quantify stiffness by measuring the mobile platform-compliant displacements

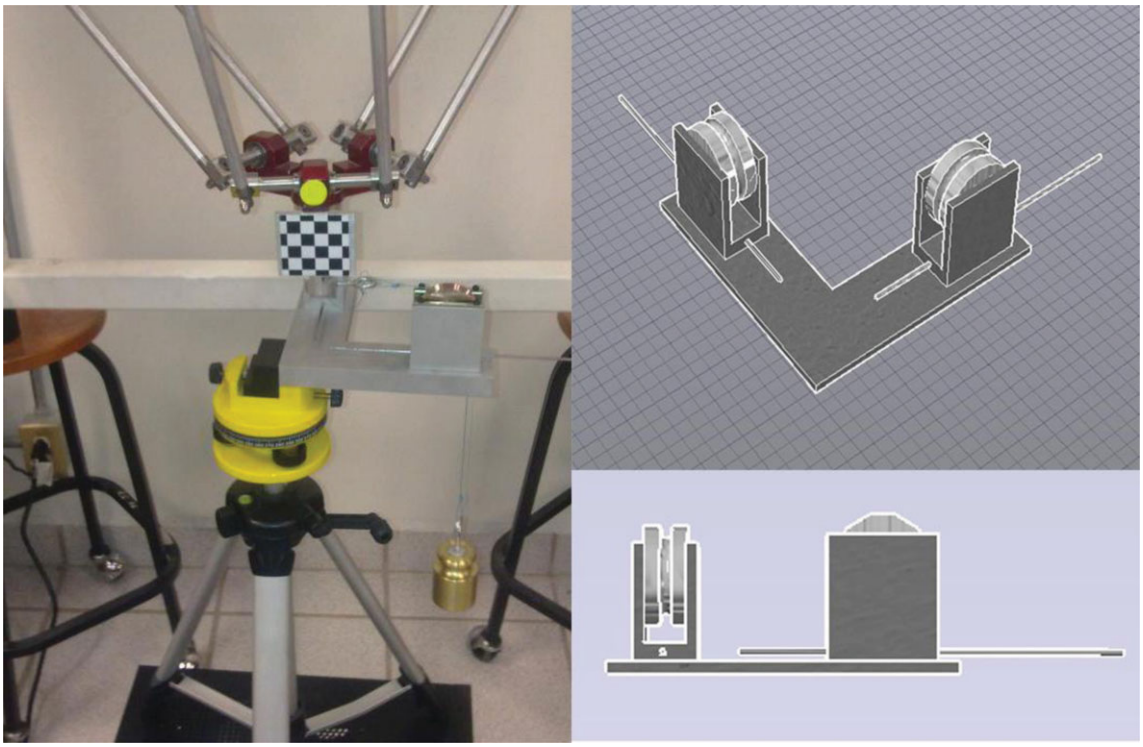

Fig. 4. (Colour online) Device for the application of known forces.

https://doi.org/10.1017/S0263574712000641 Published online by Cambridge University Press

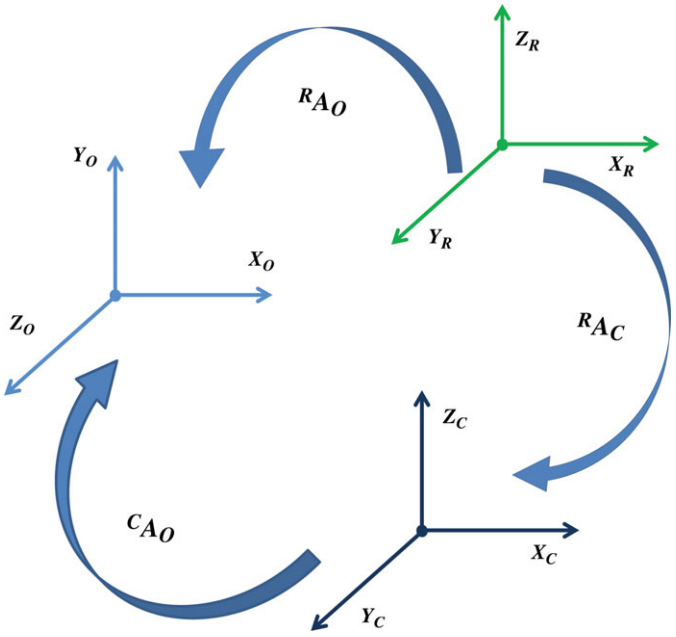

Fig. 5. (Colour online) The involved frames to estimate transformation matrix.

using image analysis. The first step is to determine the homogeneous transformation matrix that describes the coordinates of a fixed pattern (object) on robot frame. Figure 5 shows how the involved frames are related. According to Fig. 5, the homogeneous transformation matrix ^RA_C, which relates the camera frame with the robot frame, is obtained from

$$^R\boldsymbol{A}_C = {}^R\boldsymbol{A}_O^O\boldsymbol{A}_C, \tag{1}$$

where:

$^R\boldsymbol{A}_O$: Homogeneous transformation matrix of the pattern (object) with respect to robot frame;

$^O\boldsymbol{A}_C$: Homogeneous transformation matrix of the camera with respect to object frame.

The position and orientation of the fixed pattern (object) are contained in the homogeneous matrix $^C\boldsymbol{A}_O$ and these can be extracted directly as a result of the camera calibration software using the extrinsic parameters ($R_{3\times3}$ and $T_{1\times3}$) of the fixed pattern

$$^C\boldsymbol{A}_O = \begin{bmatrix} R_{3\times3} & T_{1\times3} \\ 0_{3\times1} & 1 \end{bmatrix}. \tag{2}$$

Figure 6 shows the selected plane of the object to estimate its extrinsic parameters. The matrix $^O\boldsymbol{A}_C$ is obtained using: $^O\boldsymbol{A}_C = (^C\boldsymbol{A}_O)^{-1}$. Since the pattern is fixed to the motor support, we are assuming that elements of $^R\boldsymbol{A}_O$ are constants and known from robot base geometry. However, two sources of error are possible, but we neglected both of them: (1) the machining process to build motor support, which is less than 0.05 mm (accuracy of the milling to machine that piece), and (2) the montage of motor support that is also related with milling accuracy. For this study, the homogenous matrix corresponding to the base of the servomotor 1 with respect to robot frame is as follows:

$$^R\boldsymbol{A}_O = \begin{bmatrix} 1 & 0 & 0 & -75.63 \\ 0 & 0 & 1 & 188.10 \\ 0 & -1 & 0 & 31.00 \\ 0 & 0 & 0 & 1 \end{bmatrix}.$$

3.2. Validation of displacement estimation using image analysis

To quantify the accuracy of the technique to estimate displacements of mobile pattern through image analysis, some experiments were performed by mounting a similar

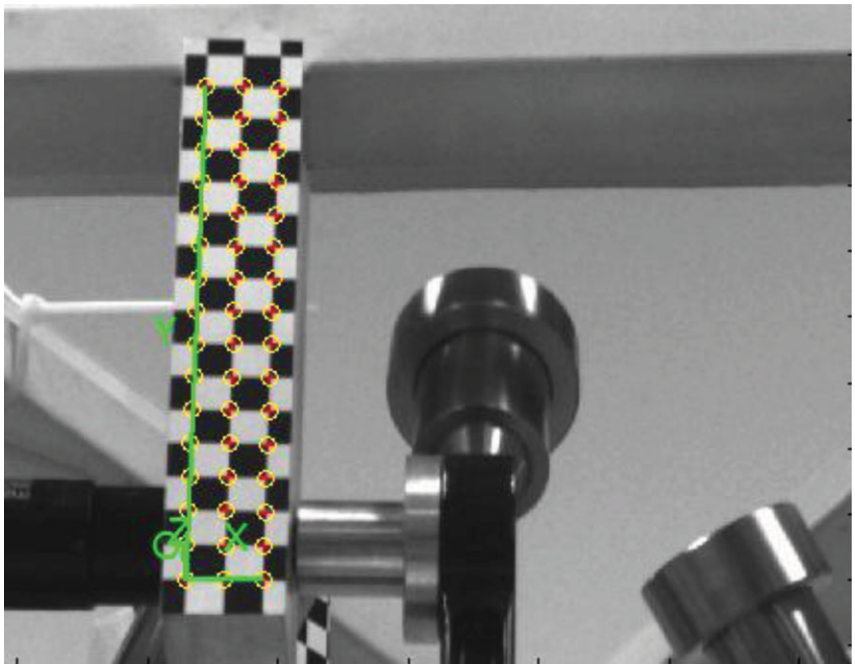

Fig. 6. (Colour online) Selected plane to estimate extrinsic parameters of the fixed pattern.

https://doi.org/10.1017/S0263574712000641 Published online by Cambridge University Press

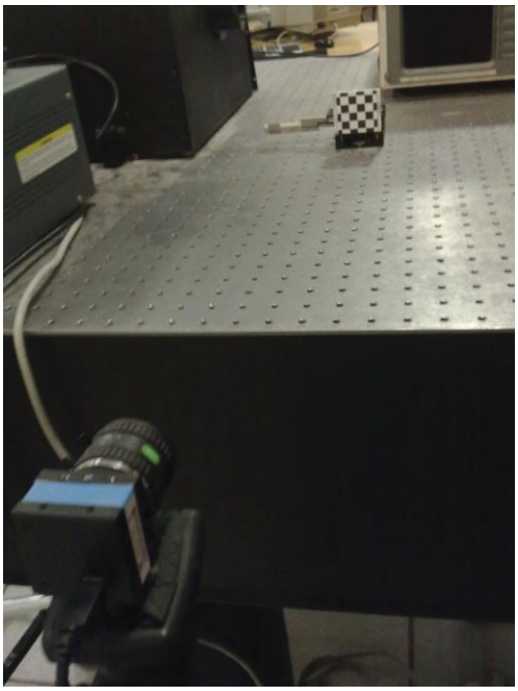

Fig. 7. (Colour online) Experimental validation using an optical X-table.

Table I. Experimental validation result.

Micrometer displacement (mm)	Estimated displacement (mm)
2	1.99 ± 0.28
5	4.97 ± 0.27
10	9.75 ± 0.24
20	20.01 ± 0.21

pattern on an optical X-table driven by a micrometer (see Fig. 7).

The pattern was displaced 2, 5, 10, and 20 mm using the micrometer of the optical X-table. Using the camera calibration techniques described previously, the extrinsic parameters of the mobile pattern were extracted. According to International Organization for Standardization's ISO 5725-1:1994,[20] 10 repeated measurements of the pattern position were performed; the repeated measurements help to estimate standard deviation reported in Table I.

In measuring tasks using cameras, it is not necessary to align them on a predetermined axis. Instead, it is preferred to "rectify" the acquired images through the calibration process as presented in refs. [21, 22]. Then the camera frame with respect to real world frame, in our case with the optical X-table frame, can be found indirectly. From the viewpoint of optical X-table, movement is 1D (driven by micrometer), but from camera frame viewpoint, it is a 3D movement. In this way the measured displacement of the optical X-table using the camera is vector $(\delta x, \delta y, \delta z)$ of displacements (extracted from camera extrinsic parameters), the estimated displacements shown in Table I correspond to the norm of this vector.

3.3. Estimation of mobile pattern-compliant displacements

Two images are required to estimate displacement when a known load is applied on the mobile platform. The first image corresponds to the pattern without load on the mobile platform; the second image corresponds with load on the mobile platform. From each image, extrinsic parameters using camera calibration can be obtained. The extrinsic parameters are the rotation matrix and the translation vector ($R_{3\times3}$ and $T_{1\times3}$) of the mobile pattern with respect to camera frame.

From the rotation matrix,

$$R = \begin{bmatrix} U_x & V_x & W_x \\ U_y & V_y & W_y \\ U_z & V_z & W_z \end{bmatrix},$$

the Euler angles can be calculated as follows:

$$\psi = \tan^{-1}\left(\frac{V_z}{W_z}\right), \tag{3}$$

$$\phi = \sin^{-1}(-U_z), \tag{4}$$

$$\theta = \tan^{-1}\left(\frac{U_y}{U_x}\right), \tag{5}$$

where:

ψ: rotation around X-axis
ϕ: rotation around Y-axis
θ: rotation around Z-axis

Moreover, from the translation vector, $T = [\, Px \;\; Py \;\; Pz \,]^t$, it is obtained directly with the pattern position for each axis.

Finally, the difference between extrinsic parameters of each of the two images corresponds to compliant displacement (three angular and three linear compliant displacements) caused by load application:

$$\begin{aligned} \delta\psi &= \psi_L - \psi_{NL} \\ \delta\phi &= \phi_L - \phi_{NL} \\ \delta\theta &= \theta_L - \theta_{NL} \\ \delta x &= Px_L - Px_{NL} \\ \delta y &= Py_L - Py_{NL} \\ \delta z &= Pz_L - Pz_{NL} \end{aligned}, \tag{6}$$

where NL = no load and L = load.

3.4. Stiffness estimation approach

In the most general case, the methodology presented in this work allows the estimation of the stiffness matrix of a manipulator, defined in ref. [10], by the following expression:

$$W = K\,\Delta\,S, \tag{7}$$

where:

K: Stiffness matrix 6×6;
ΔS: Compliant displacements of mobile platform, and $\Delta S = (\Delta x,\ \Delta y,\ \Delta z,\ \Delta\psi,\ \Delta\phi,\ \Delta\theta)$;
W: Static wrench acting on mobile platform, and $W = (Fx, Fy, Fz, Tx, Ty, Tz)$.

https://doi.org/10.1017/S0263574712000641 Published online by Cambridge University Press

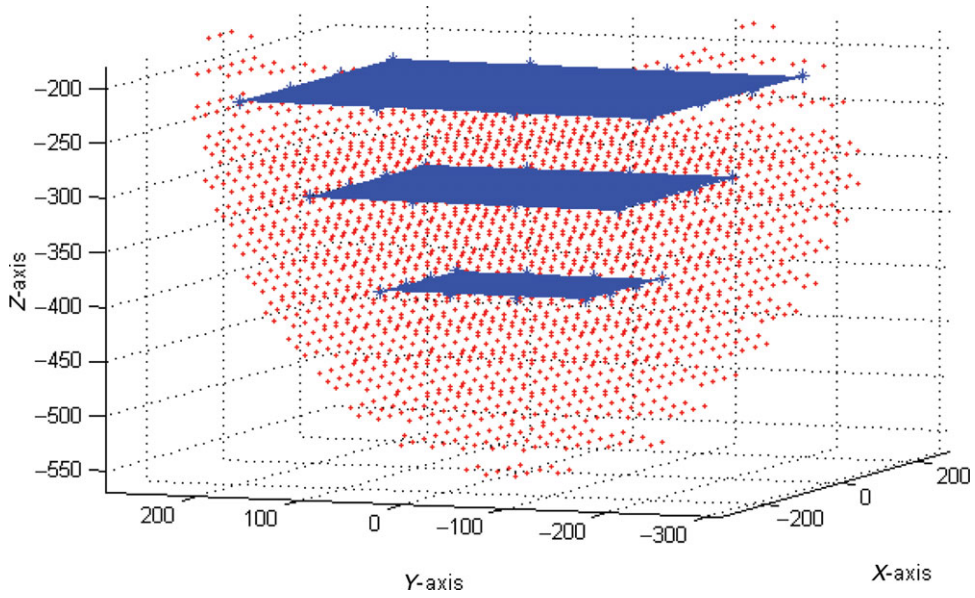

Fig. 8. (Colour online) Set of positions in millimeter where the stiffness was estimated.

Table II. Forces applied to the mobile platform.

i	F_{xi} [N]	F_{yi} [N]	F_{zi} [N]
1	0	4.905	0
2	−4.905	0	0
3	0	0	−4.905
4	0	1.962	0
5	−1.962	0	0
6	0	0	−1.962
7	0	0.981	0
8	−0.981	0	0
9	0	0	−0.981

However, since the robot under study is a translational one, we only use compliant linear displacement and forces acting on *X*–*Y*–*Z* axes at the mobile platform level:

$$F = K\delta. \tag{8}$$

In this case the stiffness matrix K is only 3×3 and can be represented by

$$K = \begin{bmatrix} k_{11} & k_{12} & k_{13} \\ k_{21} & k_{22} & k_{23} \\ k_{31} & k_{32} & k_{33} \end{bmatrix}. \tag{9}$$

The unknown coefficients of the stiffness matrix are nine, and then at least nine different forces are required to estimate them. In this way, the forces matrix F, and the compliant linear displacements δ are, respectively, as follows:

$$F = \begin{bmatrix} F_{x1} & F_{x2} & F_{x3} & F_{x4} & F_{x5} & F_{x6} & F_{x7} & F_{x8} & F_{x9} \\ F_{y1} & F_{y2} & F_{y3} & F_{y4} & F_{y5} & F_{y6} & F_{y7} & F_{y8} & F_{y9} \\ F_{z1} & F_{z2} & F_{z3} & F_{z4} & F_{z5} & F_{z6} & F_{z7} & F_{z8} & F_{z9} \end{bmatrix},$$

$$\delta = \begin{bmatrix} \delta_{x1} & \delta_{x2} & \delta_{x3} & \delta_{x4} & \delta_{x5} & \delta_{x6} & \delta_{x7} & \delta_{x8} & \delta_{x9} \\ \delta_{y1} & \delta_{y2} & \delta_{y3} & \delta_{y4} & \delta_{y5} & \delta_{y6} & \delta_{y7} & \delta_{y8} & \delta_{y9} \\ \delta_{z1} & \delta_{z2} & \delta_{z3} & \delta_{z4} & \delta_{z5} & \delta_{z6} & \delta_{z7} & \delta_{z8} & \delta_{z9} \end{bmatrix}.$$

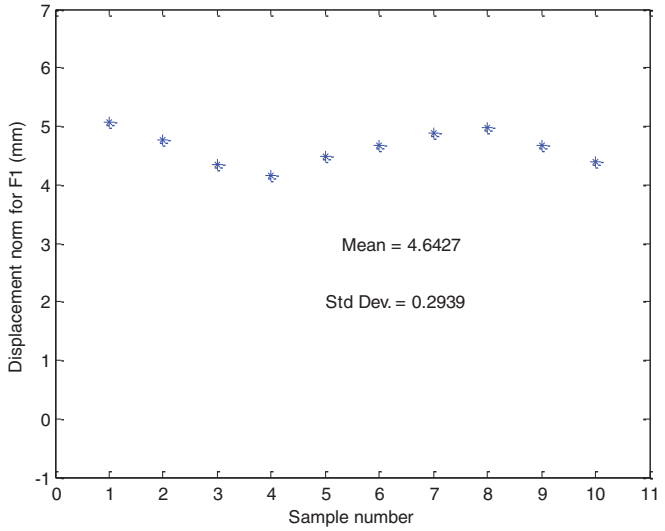

Fig. 9. (Colour online) Example of mean value and standard deviation for 10 compliant displacements.

The equation for estimating the stiffness matrix is solved by least squares method since δ is not square:

$$K = F\delta'(\delta\delta')^{-1}, \tag{10}$$

Where δ' is the transpose of matrix δ. The experimental test consists of simultaneously measuring of applied forces and corresponding compliant displacements. Moreover, the determinant of the stiffness matrix was used to quantify with a single value of stiffness in different positions of the workspace.

4. Robot Stiffness Estimation

The stiffness was computed for a set of 48 positions within the workspace of robot Parallix LKF-2040. The 48 positions are located on three planes at different Z levels –200,

https://doi.org/10.1017/S0263574712000641 Published online by Cambridge University Press

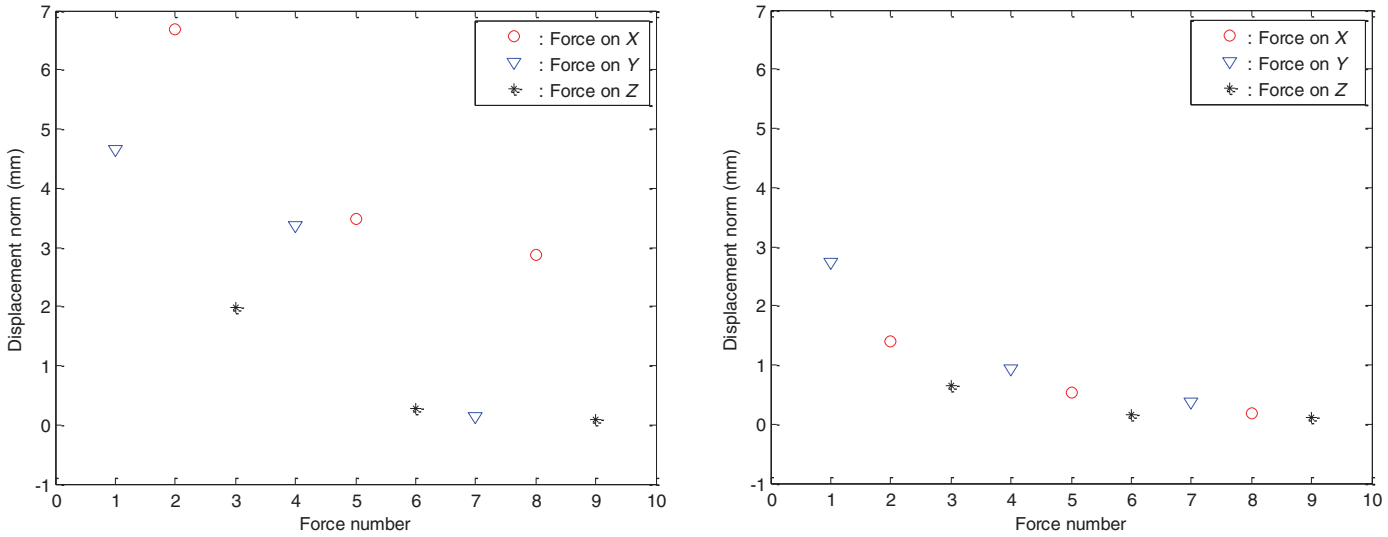

Fig. 10. (Colour online) Displacements considering nine forces for robot positions: (a) (–100, –100, –400) and (b) (150, 50, –310).

–310, and –400; each plane contains 16 positions spaced equally. The robot reference frame is located at position (0, 0, 0), which corresponds to the center of fixed platform. Figure 8 shows the robot workspace (red dots) and the set of positions (including their corresponding plane in blue) where the stiffness was estimated.

For each position, two images of the mobile pattern were acquired. These images correspond to compliant displacements generated by applying nine vector forces, shown in Table II, that correspond to a combination of three loads. The scalar forces applied are 4.905, 1.962, and 0.981 N that correspond to loads of 500, 200, and 100 g. We considered convenient to apply forces of less than 600 g, which is the maximum payload of the robot.

We are assuming that a compliant displacement occurs only when an external load is applied to the mobile platform.

Ten repeated measurements of the compliant displacement were performed for each position according to ISO 5725.[20] As an example, Fig. 9 shows 10 repeated measurements corresponding to the compliant displacement norm when force 1 (4.905 N along *Y*-axis, see Table II) is applied on the mobile platform position (–100, –100, –400). Displacement norm mean values and the corresponding standard deviations are also indicated in Fig. 9.

Figure 10 shows the compliant displacement norm corresponding to two of the 48 robot positions (–100, –100, –400) *y* (150, 50, –310), when the nine forces (see Table II), are applied to the mobile platform.

Figure 10(a) shows that the largest compliant displacement occurs when forces are applied along the *X*-axis, while the smaller one is obtained when the force is applied on the *Z*-axis. In fact, compliant displacements produced by forces of magnitude of 0.981 N on the *Y* and *Z*-axes are less than 0.3 mm. In Fig. 10(b), lower compliant displacements are observed, indicating that the stiffness is larger for that position of the mobile platform.

The stiffness numerical values presented in Table III were estimated using the mean value of compliant displacement

Table III. Stiffness matrices and determinants for six-robot positions.

		$K =$	−0.2409	0.2612	0.2029		
1	[–100, –100, –400]		0.9153	0.244	0.6019	$\Delta =$	0.6521
			0.0759	0.3547	−1.7682		
		$K =$	0.6432	1.9244	−0.7547		
2	[–100, –34, –400]		1.4974	0.9834	1.1074	$\Delta =$	10.4954
			−0.3293	0.3176	−5.3474		
			−1.7344	3.6163	−2.0876		
3	[150, 50, –310]	$K =$	1.4329	−0.2791	0.438	$\Delta =$	38.4635
			1.3356	−2.4109	−6.7579		
			−1.1034	3.3137	−1.5047		
4	[150, 150, –310]	$K =$	1.8491	−0.2564	1.0873	$\Delta =$	43.6104
			−1.4914	−1.4825	−7.8815		
			3.4201	0.2397	0.4399		
5	[–200, 200, –220]	$K =$	2.2007	0.2391	−2.4562	$\Delta =$	−4.4748
			4.1906	0.0341	−6.4945		
			0.7342	1.2172	−4.8496		
6	[200, –200, –220]	$K =$	1.2115	−0.0114	1.1727	$\Delta =$	−0.8527
			0.0378	1.207	−4.8725		

https://doi.org/10.1017/S0263574712000641 Published online by Cambridge University Press

Fig. 11. (Colour online) Some positions where the stiffness was estimated.

for each position, and the corresponding determinant of the stiffness matrix was computed. To illustrate the results obtained, some stiffness matrices and the corresponding determinants are presented in Table III. Some pictures corresponding to the acquired images are shown in Fig. 11.

5. Results

The resulting intrinsic parameters of camera calibration were used along the experimental procedure. These parameters change only if the camera optics is modified. Table IV shows intrinsic parameters values calculated and used to compute extrinsic parameters.

Figure 12 shows a stiffness map, it means a graphical representation of the robot stiffness, considering the 48 selected positions. The circle diameters are proportional to the determinant of stiffness matrix.

The stiffness estimation was performed starting from the lower level, at the coordinates [–100, –100, –400]. Stiffness is higher in the center than in the border of the workspace, as according to Yoon *et al.*,[9] a higher determinant value means higher stiffness.

At coordinates [–67, 66, –220], the highest determinant was found to be 873.27, this position is located at the center of the upper plane. It is also noted that coordinates [–200, 200, –220] and [–200, 200, –220] have the lowest values. In fact, these positions are located in the corners of the upper

Table IV. Intrinsic parameters of the camera.

Intrinsic parameters	Values
Focal distance	$[Df_x = 3733.27,\ Df_y = 3722.85] \pm [39.9636.86]$
Principal point	$[u_0 = 1466.77,\ v_0 = 904.81] \pm [24.6540.23]$
Lens distortion	$[D_1 = -0.09,\ D_2 = 0.11] \pm [0.00110.04632]$

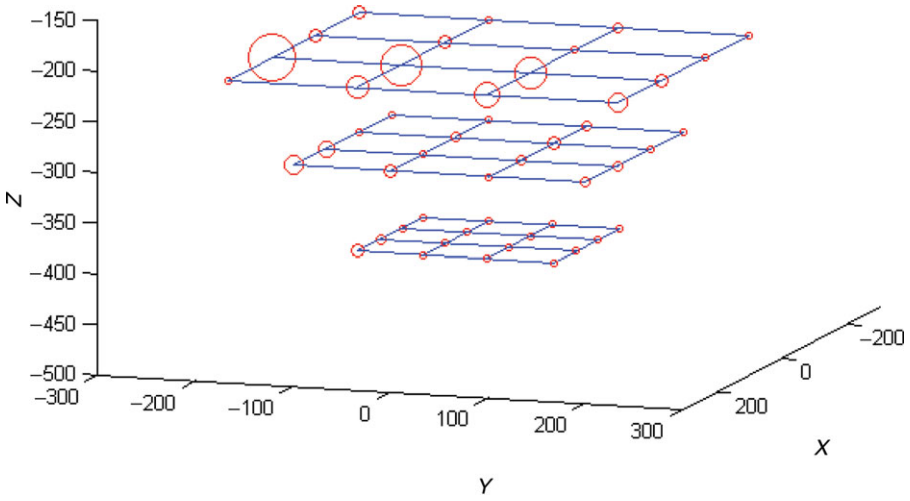

Fig. 12. (Colour online) Stiffness map of the Parallix LKF-2040 robot.

https://doi.org/10.1017/S0263574712000641 Published online by Cambridge University Press

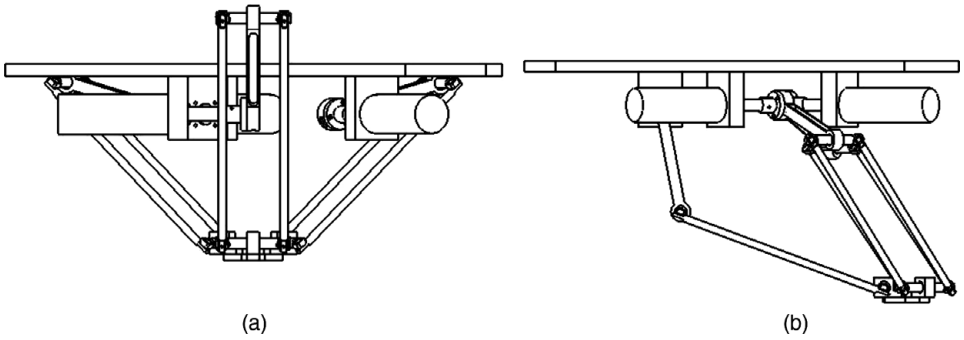

Fig. 13. (a) Links folded, configuration related with high stiffness; (b) two links extended, configuration related with low stiffness.

plane. It is important to comment that low stiffness coincides with low stability from the robot control viewpoint.

A mechanical structure is stable if the determinant of the stiffness matrix is nonzero. Therefore, the more close to zero is the determinant, less stiff will be the manipulator.

Figure 13 shows that the highest stiffness is obtained in the upper workspace, which corresponds to a configuration where the links of the robot are folded (see Fig. 13(a)).

This coincides with a common sense: man with folded elbows can support a load more rigidly.

Furthermore, the stiffness of the manipulator is low in positions away from the center of the workspace, especially at the boundaries. This can be explained because in that configuration control is less effective in maintaining the desired position, as the lever arm is higher for one or two actuators simultaneously and high torques are required. In the configuration with 1 or 2 links extended (Fig. 13(b)) the parallel manipulator presents the same disadvantages as a serial-type robot manipulator arm.

6. Conclusions

In this paper, a methodology was developed and implemented for estimating the stiffness of a parallel manipulator using image analysis techniques. The methodology was tested on a parallel robot, Parallix LKF-2040, built at IPN-CICATA, Mexico. Three different loads in *X–Y–Z* axes were applied to the mobile platform to produce compliant displacements using a home-made device for force applications. This device presented friction at pulleys level that was neglected during the experiment, the force-applied losses were experimentally estimated and were less than 6% of the applied force.

The displacement estimation using camera calibration techniques was validated experimentally. The stiffness was determined for different positions within the workspace of the robot. The determinant of the stiffness matrix was used to represent stiffness map graphically. The stiffness map shows that stiffness decreases in extreme positions of the workspace where the robot control performances decrease.

We are assuming that it is not necessary to measure angular displacements, since Delta-type robot has only translation motions. However, our approach allows extracting them for camera extrinsic parameters in case they should be considered for different robot architectures. This method proved to be practical and fast to find compliant displacements on the mobile platform when a load is applied. It can be adapted to serial robot manipulators where conventional methods to estimate stiffness are difficult to implement. The idea of stiffness map for graphical representation of robot stiffness should be studied extensively. The accuracy of this method depends on the quality of machine vision system, that is, on camera calibration technique and camera resolution. The software used in this work is based on MATLAB ToolBox "Camera Calibration Toolbox", and the camera resolution is 2592 × 1944 pixels, which allows to ensure enough accuracy for such kind of robot-compliant displacements.

Compared with other techniques to estimate stiffness in robot manipulators, the method presented in this paper has the following advantages:

- This avoids the analysis of rigidity of each one of the elements (links and joints) of the robot.
- No need to know the mechanical properties of the elements of the robot.
- The stiffness can be evaluated in all directions (translation and orientation).
- Possibility of mapping the actual stiffness for any set of robot workspace.
- Stiffness can be mapped during the execution of a given task and then compare the results under different load conditions.
- It can be used to experimentally validate theoretical stiffness analysis.
- This is a low cost method since it only requires printed patterns, a medium resolution camera, and a simple system to apply known forces.

Acknowledgments

This study was financially supported by Instituto de Ciencia y Tecnología del Gobierno del Distrito Federal, Mexico (ICYT-DF), and the authors wish to express their gratitude.

References

1. E. Castillo, "Development of parallel robots for teaching Mechatronics and Robotics", Final report, project sponsored by ICTY-DF, Mexico (2008).
2. L.-W. Tsai, *Robot Analysis: The Mechanics of Serial and Parallel Manipulators* (Jonh Wiley, 1999).
3. C. M. Gosselin, "Stiffness mapping for parallel manipulators," *IEEE Trans. Robot. Autom.* **6**, 377–382 (1990).

https://doi.org/10.1017/S0263574712000641 Published online by Cambridge University Press

4. C. M. Clinton and Y G. Zhang, "Stiffness modeling of a Stewart platform-based milling machine," *Trans. North Am. Manuf. Res. Inst. SME*, **25**, 335–340 (1997).
5. E. Rebeck and G. Zhang, "A method for evaluating the stiffness of a Hexapod machine tool support structure," *Int. J. Flexible Autom. Integr. Manuf.* **7**, 149–165 (1999).
6. T. Huang, X. Zhao and D. J. Whitehouse, "Stiffness estimation of a tripod-based parallel kinematic machine," *IEEE Trans. Robot Automat.* **18**, 50–58 (2002).
7. M. Ceccarelli and G. Carbone, "A stiffness analysis for CaPaMan (Cassino Parallel Manipulator)," *Mech. Mach. Theory* **37**, 427–439 (2002).
8. G. Carbone, M. Ceccarelli and M. Teolis, "A Numerical Evaluation of the Stiffness of CaHyMan (Cassino Hybrid Manipulator)," **In**: *Proceedings of 2nd Workshop on Computational Kinematics* (CK 2001), Seoul (2001) pp. 145–154.
9. W. K. Yoon, T. Suehiro, Y. Tsumaki and M. Uchiyama, "Stiffness analysis and design of a compact modified delta parallel mechanism," *Robotica* **22**, 463–475 (2004).
10. M. Ceccarelli and G. Carbone, "Numerical and Experimental Analysis of the Stiffness Performances of Parallel Manipulators," *Proceedings of the 2nd International Colloquium "Collaborative Research Centre 562*," Braunschweig, Germany (2005).
11. O. Company, F. Pierrot and J. C. Fauroux, "A Method for Modeling Analytical Stiffness of a Lower Mobility Parallel Manipulator," *Proceedings of the IEEE International Conference on Robotics and Automation*, Barcelona, Spain (2005).
12. C. Corradini, J. C. Fauroux, S. Krut and O. Company, "Evaluation of a 4 Degree of Freedom Parallel Manipulator Stiffness," *Proceedings of the 11th World Congress in Mechanism and Machine Science*, Tianjin, China (2004).
13. D. Deblaise, X. Hernot and P. Maurine, "A systematic analytical method of PKM stiffness matrix calculation," *Proceedings of the 2006 IEEE International Conference on Robotics and Automation*, Orlando, Florida, USA (2006).
14. F. Majou et al., "Parametric stiffness analysis of the Orthoglide," *Mech. Mach. Theory* **42**, 296–311 (2007).
15. R. S. Goncalves and J. C. Mendes Carvalho, "Stiffness Analysis of Parallel Manipulator Using Matrix Structural Analysis," **In:** *Proceedings of the Second European Conference on Mechanism Science* (EUCOMES 08) (2008) pp. 255–262.
16. A. Pashkevich, D. Chablat and P. Wenger, "Stiffness analysis of overconstrained parallel manipulators," *Mech. Mach. Theory* **44**, 966–982 (2009).
17. J. Najera, J. Aginaga and I. Zabalza, "Análisis de Rigidez de Manipuladores Paralelos Basado en el Análisis de Sensibilidad. Aplicacion al 6-RUS," *Proceedings of the 9 Congreso Iberoamericano de Ingeniería Mecánica*, Las Palmas de Gran Canaria, Spain (2009).
18. J. Lang, D. K. Pai and R. J. Woodham, "Robotic acquisition of deformable models," *IEEE Int. Conf. Robot. Autom.* **1**, 933–938 (2002).
19. J. Y. Bouguet, "Camera calibration toolbox for Matlab," Available at: http://www.vision.caltech.edu/bouguetj/calib_doc/ (2010). (Accessed 26 October 2012).
20. International Organization for Standardization, "*ISO 5725-1:1994. Accuracy (Trueness and Precision) of Measurement Methods and Results – Part 1: General Principles and Definitions*," (ISO, Geneva, Switzerland,1994).
21. Z. Zhang, "A flexible new technique for camera calibration," *IEEE Trans. Pattern Anal. Mach. Intell.* **22**(11), 1330–1334 (2000).
22. J. Heikkila and O. Silven, "A Four-Step Camera Calibration Procedure with Implicit Image Correction," **In:** *Proceedings of IEEE Computer Society Conference on Computer Vision and Pattern Recognition* (Jun. 17–19, 1997) pp. 1106–1112.

https://doi.org/10.1017/S0263574712000641 Published online by Cambridge University Press